Study on the influences of X Ray Scattering on radioscopic inspection

M. Wozniak Co-Author, J. Torrent Co-Author , A. Bancelin Co-Author (trainee)

SNECMA NDE Department Laboratory , France, Evry Corbeil, Street Auguste Desbruères, BP81 91003 EVRY CEDEX, Phone +33 1 69 87 74 40, Fax +33 1 69 87 79 81,
myriam.wozniak@snecma.fr, jacques.torrent@snecma.fr

Abstract: This study issued from European project "Verdict" (Virtual Evaluation and Robust Detection for engIne Components non destructive Testing), aimed at developing and evaluating X Ray Non Destructive Method simulation. An qualitative appreciation and quantification for X Ray scattering for modelling (SINDBAD software) was identified. The effect of such radiation on radiogram results in a disturbing blur for interpretation of indications. The method and the results described are innovative in the analysis of X Ray scattering because for aeronautic field, the configurations used with this energy range are breakthrough. The approach followed consists in an experimental and practical method for evaluating scattered radiation on final image issued from the inspection. Experimental tests results confirmed that the influence of scattering radiation are linked to density variation, geometry of parts in the axe of direct radiation and spatial area. This study performed in industrial configurations contributed to improve X Ray scattering understanding.

Keywords: scattered radiation

1 Introduction

An X-Ray radiographic image is generated by both uncollided and scattered photons. Only the uncollided photons contribute to the exploitable part of radiographs, with the sharp structures of the examined parts. On the other hand, scattered radiation generated inside an object may have significant deleterious effects on image quality. Contribution of scattering to the photon intensity may vary from a few percent of the overall beam incident upon the detector to more than half of the overall beam intensity. We can denote several damaging effects of the scattered radiation :

- The scattered radiation add an important continuous component to the whole beam detected in the film. Consequently and especially for film detector, scattered radiation can induce problems of saturation and contrast.
- Depending of the equipment set-up and of the examined part, the scattered radiation component can present low frequency which disturb the radiograph.
- Finally, the scattered radiation can add important noise to the signal, which reduces the relative contrast of the flaw indication.

The facts which influence this phenomenon can be linked to the characteristics of the part tested (material, shape, thickness), to the shot parameters (energy, electronic flow, distance source-part, part-detector, angle emission-axis/detector, lead protections or not...) and to the environmental conditions of the tests.

2 Previous tests results [1]

The Canberra detector is a low energy germanium detector (LeGe) which collects X-ray radiations and discriminates them in energy. It is coupled to a SNECMA software called Spectrum Analysis Software which displays the data collected by the detector. The most useful characteristic for the current application is the surface of the spectrometric graphs.

The tests have been made on Pb part, pierced Pb part, Inconel and titanium wedges, stiffener part and fan blade.

These first experimental tests (Figure 1) had showed a contradiction with theory: the scattering due to the SN Ti part was more important when the part was at 14 cm from the detector than when it was on detector whereas it should have been the opposite results if we consider theory.
These are the results obtained for the different configurations tested:

Test type	Energy	Distance s-d/p	Distance d-p	Flow	Protection	Surface peak	% difference	comments
Direct	22,2kV	1m	-	0,25mA	none	1307857	-	
Direct	91kV+col 4,5mm	3m+col 20mm	-	0,65mA	none	2411643	30%	Protection influence
Direct	91kV+col 4,5mm	3m+col 20mm	-	0,65mA	on detector	1708911		
Direct	160kV+col 4,5mm	3m+col 20mm	-	0,2mA	none	3057097	18%	Protection influence
Direct	160kV+col 4,5mm	3m+col 20mm	-	0,2mA	on detector	2491861		
On TU part	74,2kV	1m	Config C	0,2mA	none	2820484	37%	Geometry influence
On TU part	74,2kV	1m	Config D	0,2mA	none	1791977		
On SN Ti part (s.g.)	91kV+col 4,5mm	3m+col 20mm	-	0,65mA	none	1358905	40%	Protection influence
On SN Ti part (s.g.)	91kV+col 4,5mm	3m+col 20mm	-	0,65mA	on detector	816969		
On SN Ti part (s.g.)	110kV+col 4,5mm	3m+col 20mm	-	0,65mA	none	2981198	25%	Protection influence
On SN Ti part (s.g.)	110kV+col 4,5mm	3m+col 20mm	-	0,65mA	on detector	2216143		
On SN Ti part (s.g.)	110kV+col 4,5mm	3m+col 20mm	-	0,65mA	none	2981198	697980 =19%	Distance from detector influence
On SN Ti part (s.g.)	110kV+col 4,5mm	3m+col 20mm	14cm	0,65mA	none	3679178		
Direct	91kV+col 4,5mm	3m+col 20mm	-	0,65mA	none	2411643	43%	Influence before and after part
On SN Ti part (s.g.)	91kV+col 4,5mm	3m+col 20mm	-	0,65mA	none	1358905		
On SN Ti part (s.g.)	41,6kV	1m	20cm	0,2mA	none	3297871	1%	Protection influence
On SN Ti part (s.g.)	41,6kV	1m	20cm	0,2mA	on detector	3258207		
On SN Ti part (s.g.)	41,6kV	1m	-	0,2mA	none	2469167	2%	Protection influence
On SN Ti part (s.g.)	41,6kV	1m	-	0,2mA	on detector	2422611		
On SN Ti part (s.g.)	41,6kV	1m	-	0,2mA	none	2469167	25%	Distance from detector influence
On SN Ti part (s.g.)	41,6kV	1m	20cm	0,2mA	none	3297871		
On SN inco part (s.g)	52,4kV	1m	-	0,2mA	none	551251	84%	Distance from detector influence
On SN inco part (s.g)	52,4kV	1m	20cm	0,2mA	none	3476386		
On SN inco part (s.g)	52,4kV	1m	20cm	0,2mA	none	3476386	5%	Protection influence
On SN inco part (s.g)	52,4kV	1m	20cm	0,2mA	on detector	3272693		
On SN inco part (s.g)	52,4kV	1m	-	0,2mA	none	551251	36%	Protection influence
On SN inco part (s.g)	52,4kV	1m	-	0,2mA	on detector	350716		
On SN inco part (c.g)	101kV	3m	-	0,2mA	none	3015421	62%	Energy influence

Figure 1: previous tests results

In order to check the environmental influence on scattered radiation measurement some new experimental tests were performed (see § 3).

3 New experimental tests [2]

Six positions of the Canberra detector were tested: 75°, 45°, 15°, -15°, -45° and -75° from the axis of X-ray emission. For each position, 4 shots were done with a large source: 100, 120, 140 and 160 KV with a collimator (thickness = 5 mm, hole diameter = 9 mm) against the source and no collimator on the detector.
First were performed in comparison tests on a Pb part then on a pierced Pb part. In the first case, no direct radiation can go through such a thickness of lead so the energy got by the detector in this configuration is only due to the environmental scattering. In the second configuration, the piercing is a secondary X-ray source so, the scattered radiations got by the detector come from the environmental scattering and the secondary source scattering.

3.1 Experimental evaluation on lead part

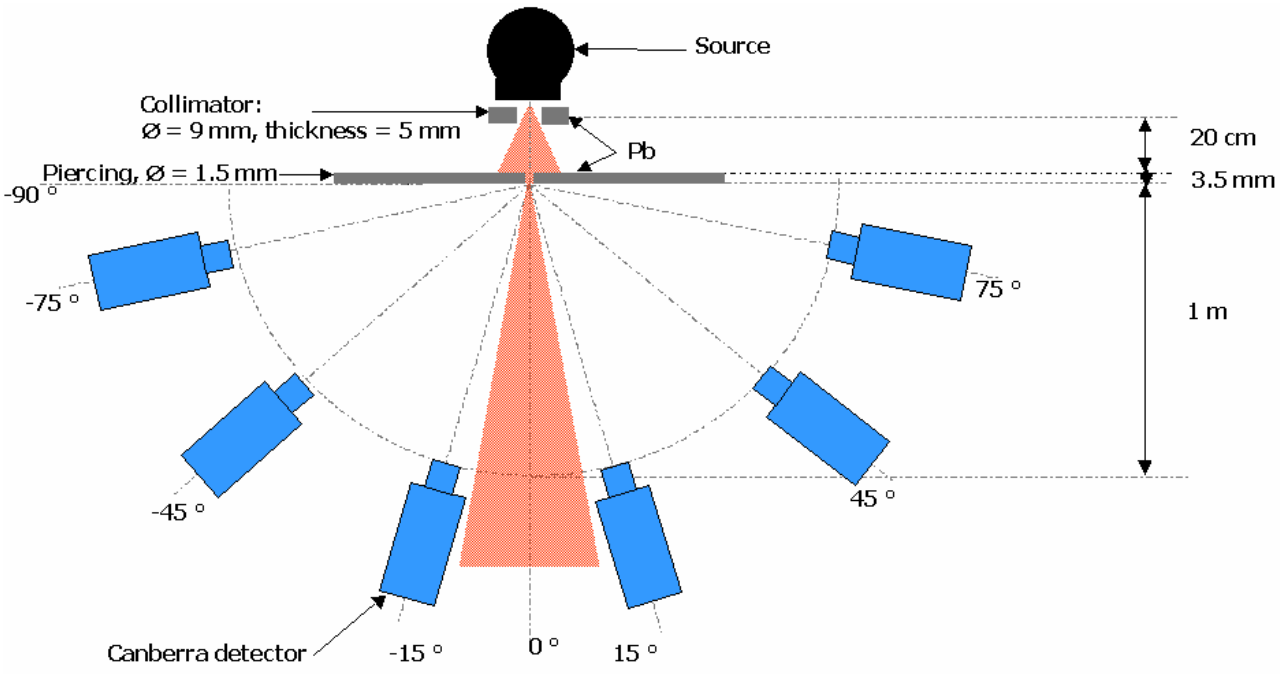

Figure 2: shots on the case of pierced Pb part

The corresponding graph (Figure 3) is following:

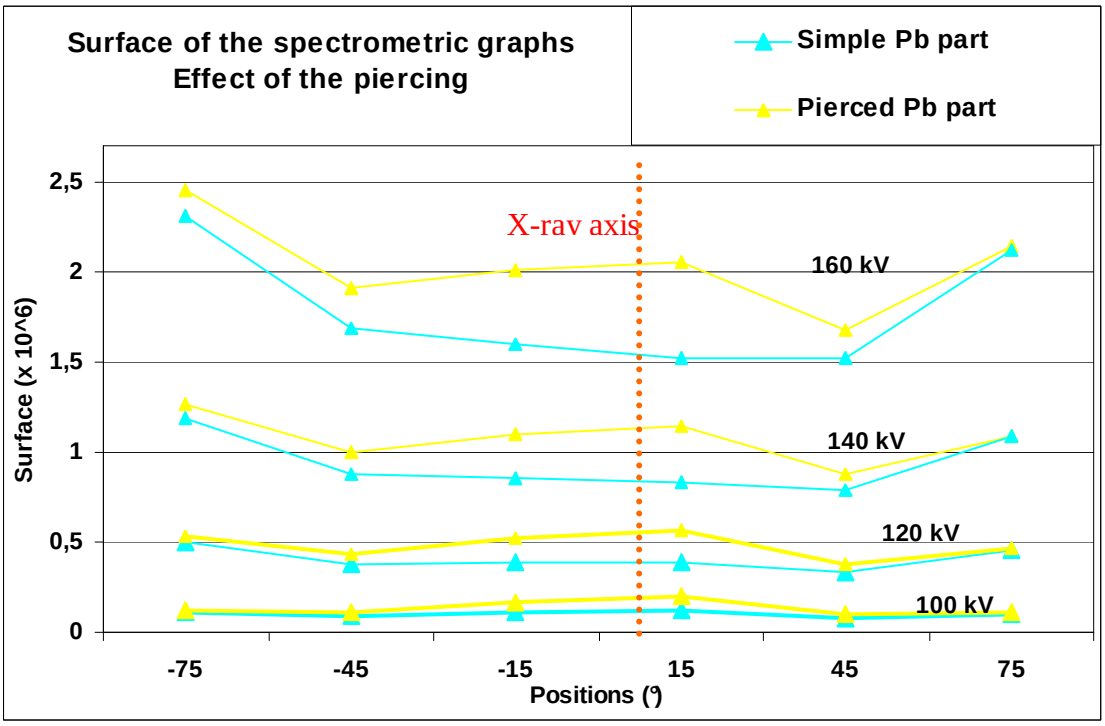

Figure 3: comparison with/without the piercing

The differences between the 2 configurations (Figure) are rather important near the X-ray axis (positions -15 & 15°) and small far from the axis (positions -75, -45, 45 & 75°).
Given that the piercing (diameter 1.5 mm) has been done on the X-ray axis, it is logical to get important change due to the secondary source scattering in positions -15/15° and little change in other positions for whom the scattering is due to the environment in the 2 configurations.

Regarding interpretation, on obtained curves:

- **Surface-flow.** While the electronic flow increases, the spectrometric surfaces increase too. The detector counts a number of hits so it is logical to have more hits with a higher flow.

- **Surface-energy**. While the energy increases, the spectrometric surfaces increase too. It is as well logical: the high energy photons are less stopped than low energy ones so they reach the detector more easily.

- **Symmetry.** The graphs are almost symmetrical from the X-ray axis; especially at low energy (100 & 120 kV). At 140 & 160 kV there is a light imbalance: the surfaces got in positions -75, -45 & -15 ° are a bit higher than the surfaces got in symmetrical positions. This can be due to the non symmetry of the X-ray source.

- **Shapes of the graphs.** At high energies (140 & 160 kV), the surfaces got in positions -75 & 75° are a lot higher than the others which are rather equal. It can be explained because -75 & 75° are the positions where the detector is the closest from the source. At 120 kV the difference between extreme positions and other one is very less important than before. At 100

kV, the reverse phenomenon is beginning: the maximum surfaces are got in central positions -15 & 15 °. At 100 & 120 kV, the graphs show minima in positions -45 & 45°.

3.2 Effect of geometry: comparison between stiffener part and Inconel wedge

This is the comparison between the surfaces got in the pierced Pb part + stiffener part configuration and in the pierced Pb part + Inconel wedge configuration for the different positions tested:

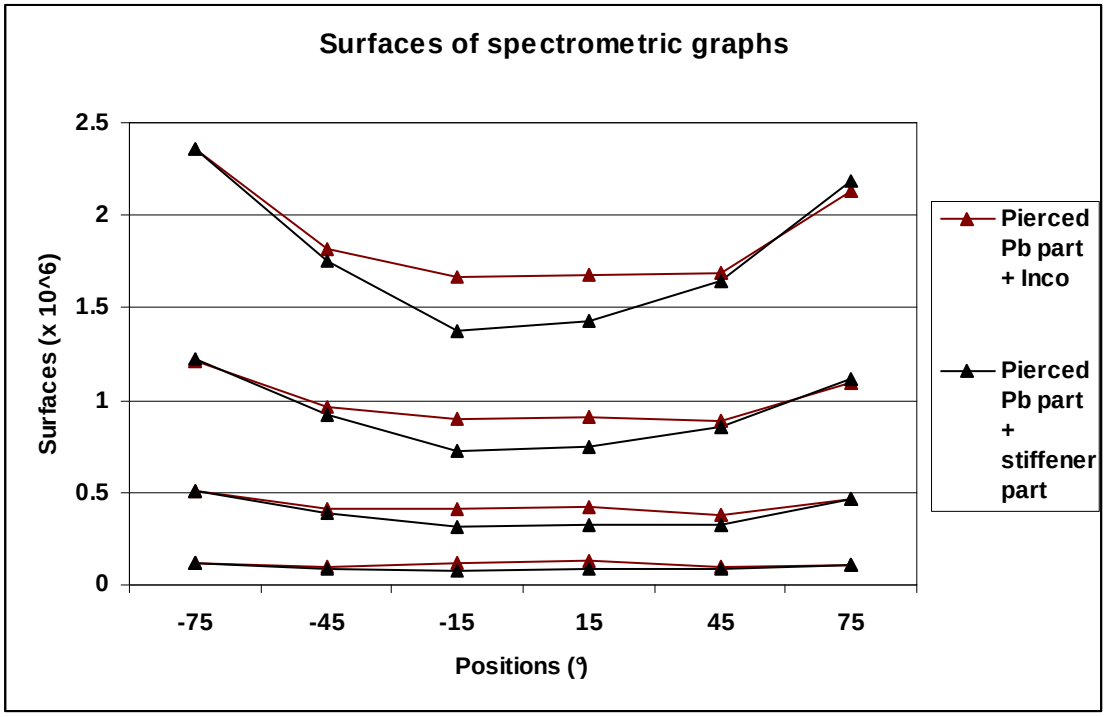

Figure 4: comparison Inconel wedge – stiffener part

The Figure 4 shows that the differences between the 2 configurations are rather important near the X-ray axis (positions -15 & 15°) and very small far from the axis (positions -75, -45, 45 & 75°).
The effect of the geometry change is visible near the X-ray axis : the surfaces got with the Inconel wedge are more important than the surfaces got with the stiffener part. The higher thickness and the complex geometry of the stiffener part is responsible for this attenuation.

Far from the X-ray axis, the environmental scattering is predominant and there is no change between the 2 configurations.

3.3 Data Recapitulation

This is the results synthesis for the configurations Pb part, pierced Pb part, pierced Pb part + Inconel wedge, pierced Pb part + stiffener part, pierced Pb part + titanium wedge and pierced Pb part + fan blade:

3.4 Comments on the shape of the graphs

Whatever the configuration, the graphs got can have 2 different shapes. There is a shape which corresponds to the position -15 & 15° (Figure 5) and an other shape to the positions -75, -45, 45 & 75° (Figure).

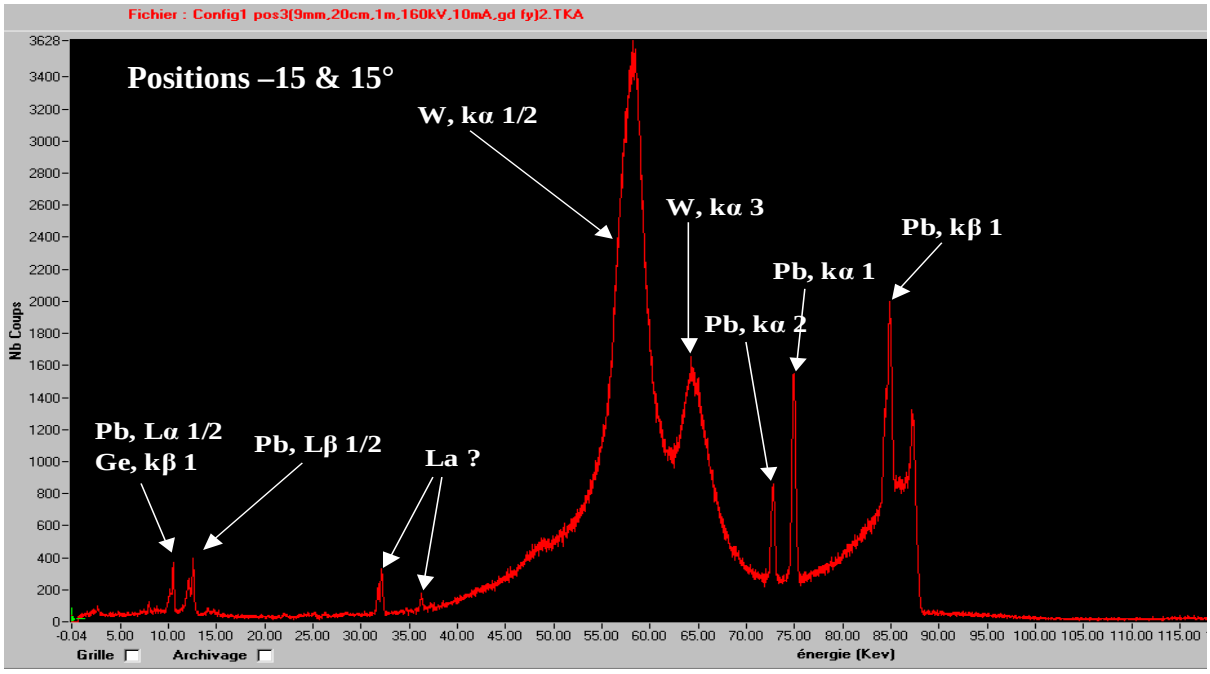

Figure 5: typical shape of the graphs in positions –15 & 15°

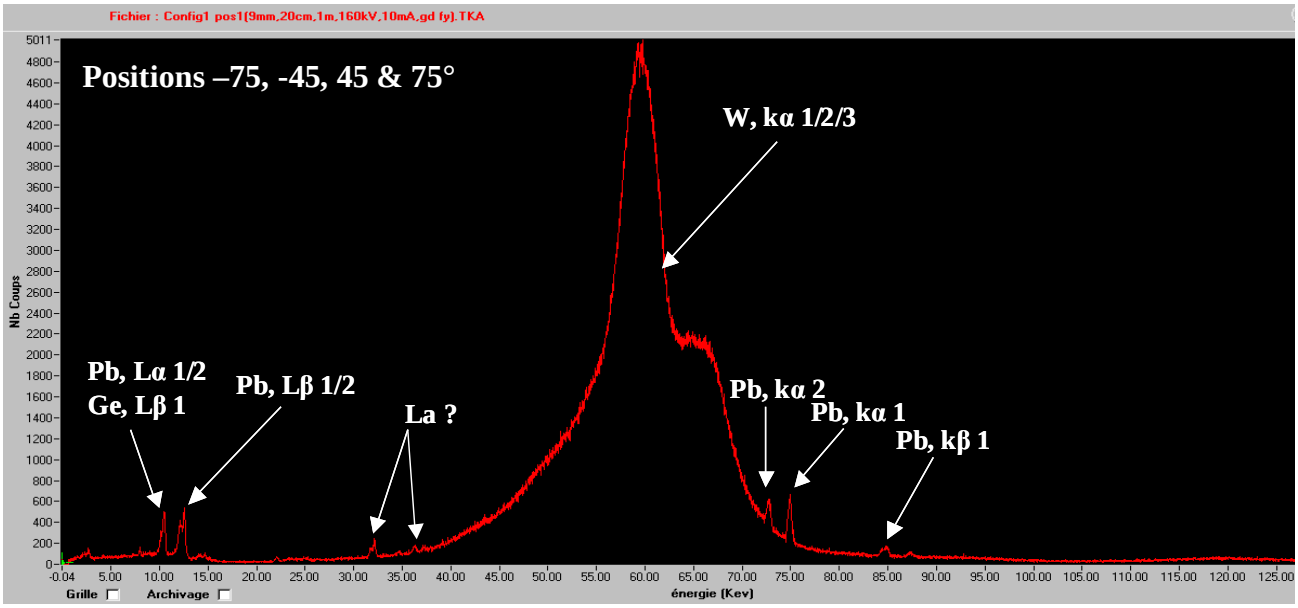

Figure 6: typical shape of the graphs in positions –75, -45, 45 & 75°

The main difference between these 2 types of graphs is the intensity of the Pb peaks Kα1, Kα2 and Kβ1 which correspond to the energy band 70 - 90 KeV. In positions -15 & 15°, these peaks are very more important (from 800 to 2000 counts) than in the other positions (from 100 to 600 counts).

4 Comparison between the different configurations

4.1 Comparative graphs

This is the synthesis of all the configurations tested:

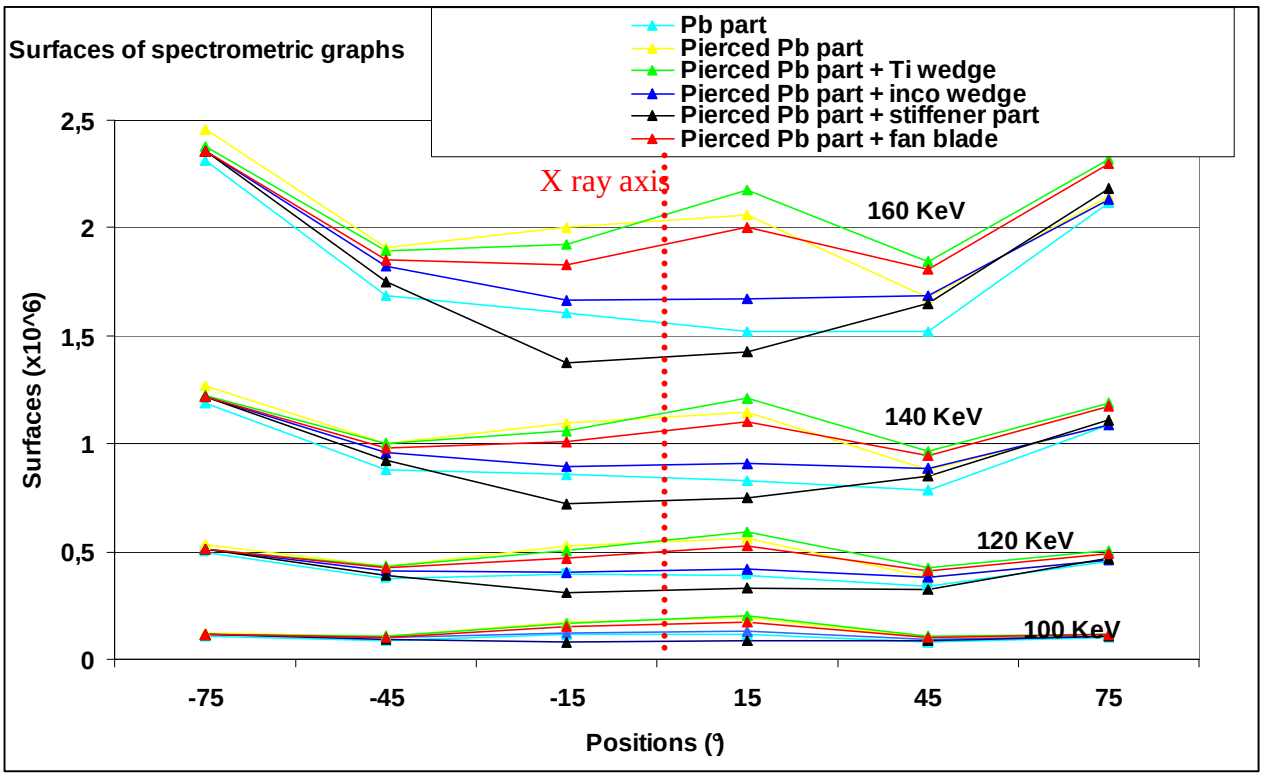

Figure 7: the 6 configurations tested

The graphs comparison (Figure 7) shows that, in positions -45 & 45° and particularly in -75 & 75°, the surfaces of all the configurations are very close. In -15 & 15°, the differences between the surfaces are important. It shows that the energy got in extreme position (-75, -45, 45 & 75°) is due to the environmental scattering which doesn't change according to the configuration whereas in the central position, the secondary source scattering and the part scattering are influential.

4.2 Environmental scattering

In the simple Pb part configuration (see 3.1), no radiation can go through the Pb thickness. So the energy got by the detector in this configuration is only due to the environmental scattering.
These are the environmental scattering values:

Angle axis-detector	Energy	Flow	Simple Pb part	Environmental scattering
-75 °	100 kV + coll 9 mm	7 mA	110651	110651
-75 °	120 kV + coll 9 mm	8 mA	497666	497666
-75 °	140 kV + coll 9 mm	9 mA	1190728	1190728
-75 °	160 kV + coll 9 mm	10 mA	2316141	2316141
-45 °	100 kV + coll 9 mm	7 mA	86940	86940
-45 °	120 kV + coll 9 mm	8 mA	374446	374446
-45 °	140 kV + coll 9 mm	9 mA	881833	881833
-45 °	160 kV + coll 9 mm	10 mA	1686811	1686811
-15 °	100 kV + coll 9 mm	7 mA	114185	114185
-15 °	120 kV + coll 9 mm	8 mA	394364	394364
-15 °	140 kV + coll 9 mm	9 mA	859694	859694
-15 °	160 kV + coll 9 mm	10 mA	1604745	1604745
15 °	100 kV + coll 9 mm	7 mA	117568	117568
15 °	120 kV + coll 9 mm	8 mA	388903	388903
15 °	140 kV + coll 9 mm	9 mA	828012	828012
15 °	160 kV + coll 9 mm	10 mA	1519536	1519536
45 °	100 kV + coll 9 mm	7 mA	80467	80467
45 °	120 kV + coll 9 mm	8 mA	337608	337608
45 °	140 kV + coll 9 mm	9 mA	787090	787090
45 °	160 kV + coll 9 mm	10 mA	1521294	1521294
75 °	100 kV + coll 9 mm	7 mA	103455	103455
75 °	120 kV + coll 9 mm	8 mA	452525	452525
75 °	140 kV + coll 9 mm	9 mA	1085348	1085348
75 °	160 kV + coll 9 mm	10 mA	2121401	2121401

Figure 8: environmental scattering values = surfaces got in simple Pb part configuration

Possible explanation for the contradiction showed in the previous tests results (Figure 1):

The difference got between the configuration “Titanium part at 14 cm from the detector” and the configuration “Titanium part on detector” could be due to the environment scattering contribution. When the part is on detector, it gets only the part scattering, but it can get the environmental scattering too when the part is 14 cm before. The environmental scattering has been estimated in the previous table (Figure 8) so it is possible to make a comparison (Figure 9):

	Previous tests : difference “part at 14 cm” - “part on detector”	New tests: environmental scattering			
Shot parameters	110 KeV, 0.65 mA	100 KeV, 7 mA		120 KeV, 8 mA	
Collimation	Ø = 4.5 mm on source Ø = 20 mm on detector	Ø = 9 mm on source		Ø = 9 mm on source	
Detector / X-ray axis	0°	-15°	15°	-15°	15°
Surfaces	697980	114185	117568	397364	388903

Figure 9: explanation for previous tests contradiction

The difference between the configuration “Titanium part at 14 cm of the detector” and the configuration “Titanium part on detector” are important but the shot parameters where rather different too (shots in position 0° in previous tests).

4.3 Secondary source scattering

The piercing in the Pb part can be considered as a secondary source. By calculating the difference between the surfaces got with the pierced Pb part and the surfaces got with the simple Pb part, it is possible to get the surfaces due to the secondary source scattering.
These are the secondary source scattering values:

Angle axis-detector	Energy	Flow	Simple Pb part	Pierced Pb part	Secondary source scattering
-75 °	100 kV + coll 9 mm	7 mA	110651	123304	12653
-75 °	120 kV + coll 9 mm	8 mA	497666	533578	35912
-75 °	140 kV + coll 9 mm	9 mA	1190728	1265553	74825
-75 °	160 kV + coll 9 mm	10 mA	2316141	2457166	141025
-45 °	100 kV + coll 9 mm	7 mA	86940	106364	19424
-45 °	120 kV + coll 9 mm	8 mA	374446	429564	55118
-45 °	140 kV + coll 9 mm	9 mA	881833	1000384	118551
-45 °	160 kV + coll 9 mm	10 mA	1686811	1912100	225289
-15 °	100 kV + coll 9 mm	7 mA	114185	172137	57952
-15 °	120 kV + coll 9 mm	8 mA	394364	522887	128523
-15 °	140 kV + coll 9 mm	9 mA	859694	1095859	236165
-15 °	160 kV + coll 9 mm	10 mA	1604745	2006219	401474
15 °	100 kV + coll 9 mm	7 mA	117568	195256	77688
15 °	120 kV + coll 9 mm	8 mA	388903	561265	172362
15 °	140 kV + coll 9 mm	9 mA	828012	1143153	315141
15 °	160 kV + coll 9 mm	10 mA	1519536	2056971	537435
45 °	100 kV + coll 9 mm	7 mA	80467	98338	17871
45 °	120 kV + coll 9 mm	8 mA	337608	381469	43861
45 °	140 kV + coll 9 mm	9 mA	787090	875718	88628
45 °	160 kV + coll 9 mm	10 mA	1521294	1680210	158916
75 °	100 kV + coll 9 mm	7 mA	103455	108612	5157
75 °	120 kV + coll 9 mm	8 mA	452525	464206	11681
75 °	140 kV + coll 9 mm	9 mA	1085348	1090492	5144
75 °	160 kV + coll 9 mm	10 mA	2121401	2144041	22640

Figure 10: secondary source scattering = difference pierced Pb part – simple Pb part

4.4 Parts scattering

The surfaces got with the parts tested take in count the part scattering, the secondary source scattering and the environmental scattering.

The subtraction of the secondary source scattering and the environmental scattering from the surfaces got with the pierced Pb part + part (Inconel & titanium wedges, stiffener part or fan blade) gives the part scattering.

4.4.1 Inconel wedge scattering

These are the Inconel wedge scattering values:

Angle axis-detector	Energy	Flow	Pierced Pb part + Inco wedge	Environmental scattering	Secondary source scattering	Inco wedge scattering
-75 °	100 kV + coll 9 mm	7 mA	117760	110651	12653	-5544
-75 °	120 kV + coll 9 mm	8 mA	512811	497666	35912	-20767
-75 °	140 kV + coll 9 mm	9 mA	1216602	1190728	74825	-48951
-75 °	160 kV + coll 9 mm	10 mA	2354852	2316141	141025	-102314
-45 °	100 kV + coll 9 mm	7 mA	100702	86940	19424	-5662
-45 °	120 kV + coll 9 mm	8 mA	410136	374446	55118	-19428
-45 °	140 kV + coll 9 mm	9 mA	957952	881833	118551	-42432
-45 °	160 kV + coll 9 mm	10 mA	1819824	1686811	225289	-92276
-15 °	100 kV + coll 9 mm	7 mA	120963	114185	57952	-51174
-15 °	120 kV + coll 9 mm	8 mA	406692	394364	128523	-116195
-15 °	140 kV + coll 9 mm	9 mA	894201	859694	236165	-201658
-15 °	160 kV + coll 9 mm	10 mA	1665152	1604745	401474	-341067
15 °	100 kV + coll 9 mm	7 mA	129235	117568	77688	-66021
15 °	120 kV + coll 9 mm	8 mA	420034	388903	172362	-141231
15 °	140 kV + coll 9 mm	9 mA	908898	828012	315141	-234255
15 °	160 kV + coll 9 mm	10 mA	1674762	1519536	537435	-382209
45 °	100 kV + coll 9 mm	7 mA	96767	80467	17871	-1571
45 °	120 kV + coll 9 mm	8 mA	382586	337608	43861	1117
45 °	140 kV + coll 9 mm	9 mA	882590	787090	88628	6872
45 °	160 kV + coll 9 mm	10 mA	1686844	1521294	158916	6634
75 °	100 kV + coll 9 mm	7 mA	107956	103455	5157	-656
75 °	120 kV + coll 9 mm	8 mA	461962	452525	11681	-2244
75 °	140 kV + coll 9 mm	9 mA	1090303	1085348	5144	-189
75 °	160 kV + coll 9 mm	10 mA	2130510	2121401	22640	-13531

Figure 11: Inconel wedge scattering

Possible explanation for negative values:
The Inconel part causes scattered radiation, but it also plays the role of a radiation filter. As a consequence, the surfaces got by the detector are less important than in the case of a total scattering. The absolute values of the results got after subtraction could represent the Inconel part maximum scattering if there were no part filtering.
When the results of the subtraction is a positive value, it shows that the filtering is weak.

4.4.2 Stiffener part scattering

These are the stiffener part scattering values:

Angle axis-detector	Energy	Flow	Pierced Pb part + Stiffener part	Environmental scattering	Secondary source scattering	Stiffener part scattering
-75 °	100 kV + coll 9 mm	7 mA	114879	110651	12653	-8425
-75 °	120 kV + coll 9 mm	8 mA	509430	497666	35912	-24148
-75 °	140 kV + coll 9 mm	9 mA	1217684	1190728	74825	-47869
-75 °	160 kV + coll 9 mm	10 mA	2356528	2316141	141025	-100638
-45 °	100 kV + coll 9 mm	7 mA	91477	86940	19424	-14887
-45 °	120 kV + coll 9 mm	8 mA	391455	374446	55118	-38109
-45 °	140 kV + coll 9 mm	9 mA	920670	881833	118551	-79714
-45 °	160 kV + coll 9 mm	10 mA	1753656	1686811	225289	-158444
-15 °	100 kV + coll 9 mm	7 mA	77679	114185	57952	-94458
-15 °	120 kV + coll 9 mm	8 mA	312086	394364	128523	-210801
-15 °	140 kV + coll 9 mm	9 mA	723765	859694	236165	-372094
-15 °	160 kV + coll 9 mm	10 mA	1376163	1604745	401474	-630056
15 °	100 kV + coll 9 mm	7 mA	85628	117568	77688	-109628
15 °	120 kV + coll 9 mm	8 mA	328789	388903	172362	-232476
15 °	140 kV + coll 9 mm	9 mA	751043	828012	315141	-392110
15 °	160 kV + coll 9 mm	10 mA	1429871	1519536	537435	-627100
45 °	100 kV + coll 9 mm	7 mA	87637	80467	17871	-10701
45 °	120 kV + coll 9 mm	8 mA	323742	337608	43861	-57727
45 °	140 kV + coll 9 mm	9 mA	852778	787090	88628	-22940
45 °	160 kV + coll 9 mm	10 mA	1649329	1521294	158916	-30881
75 °	100 kV + coll 9 mm	7 mA	107066	103455	5157	-1546
75 °	120 kV + coll 9 mm	8 mA	467671	452525	11681	3465
75 °	140 kV + coll 9 mm	9 mA	1112877	1085348	5144	22385
75 °	160 kV + coll 9 mm	10 mA	2182024	2121401	22640	37983

Figure 13: stiffener part scattering

Like in the previous case, the absolute values of the results got after subtraction could represent the stiffener part scattering if there were no part filtering.

4.4.3 Titanium wedge scattering

These are the titanium wedge scattering values:

Angle axis-detector	Energy	Flow	Pierced Pb part + Ti wedge	Environmental scattering	Secondary source scattering	Ti wedge scattering
-75 °	100 kV + coll 9 mm	7 mA	117735	110651	12653	-5569
-75 °	120 kV + coll 9 mm	8 mA	513911	497666	35912	-19667
-75 °	140 kV + coll 9 mm	9 mA	1227646	1190728	74825	-37907
-75 °	160 kV + coll 9 mm	10 mA	2379791	2316141	141025	-77375
-45 °	100 kV + coll 9 mm	7 mA	108533	86940	19424	2169
-45 °	120 kV + coll 9 mm	8 mA	432769	374446	55118	3205
-45 °	140 kV + coll 9 mm	9 mA	1000347	881833	118551	-37

Angle axis-detector	Energy	Flow	Pierced Pb part + Ti wedge	Environmental scattering	Secondary source scattering	Ti wedge scattering
-45 °	160 kV + coll 9 mm	10 mA	1894798	1686811	225289	-17302
-15 °	100 kV + coll 9 mm	7 mA	164764	114185	57952	-7373
-15 °	120 kV + coll 9 mm	8 mA	502717	394364	128523	-20170
-15 °	140 kV + coll 9 mm	9 mA	1057989	859694	236165	-37870
-15 °	160 kV + coll 9 mm	10 mA	1923654	1604745	401474	-82565
15 °	100 kV + coll 9 mm	7 mA	202855	117568	77688	7599
15 °	120 kV + coll 9 mm	8 mA	589120	388903	172362	27855
15 °	140 kV + coll 9 mm	9 mA	1208921	828012	315141	65768
15 °	160 kV + coll 9 mm	10 mA	2172776	1519536	537435	115805
45 °	100 kV + coll 9 mm	7 mA	110428	80467	17871	12090
45 °	120 kV + coll 9 mm	8 mA	423946	337608	43861	42477
45 °	140 kV + coll 9 mm	9 mA	963172	787090	88628	87454
45 °	160 kV + coll 9 mm	10 mA	1842476	1521294	158916	162266
75 °	100 kV + coll 9 mm	7 mA	115745	103455	5157	7133
75 °	120 kV + coll 9 mm	8 mA	500772	452525	11681	36566
75 °	140 kV + coll 9 mm	9 mA	1186172	1085348	5144	95680
75 °	160 kV + coll 9 mm	10 mA	2318950	2121401	22640	174909

Figure 14: titanium wedge scattering

Like in the previous case, the absolute values of the results got after subtraction could represent the titanium part scattering if there were no part filtering.
There are many positive results; it confirms that the titanium stops very few radiation.

4.4.4 Fan blade scattering

These are the fan blade scattering values:

Angle axis-detector	Energy	Flow	Pierced Pb part + Fan blade	Environmental scattering	Secondary source scattering	Fan blade scattering
-75 °	100 kV + coll 9 mm	7 mA	115226	110651	12653	-8078
-75 °	120 kV + coll 9 mm	8 mA	508915	497666	35912	-24663
-75 °	140 kV + coll 9 mm	9 mA	1215810	1190728	74825	-49743
-75 °	160 kV + coll 9 mm	10 mA	2352591	2316141	141025	-104575
-45 °	100 kV + coll 9 mm	7 mA	104127	86940	19424	-2237
-45 °	120 kV + coll 9 mm	8 mA	422282	374446	55118	-7282
-45 °	140 kV + coll 9 mm	9 mA	976935	881833	118551	-23449
-45 °	160 kV + coll 9 mm	10 mA	1854003	1686811	225289	-58097
-15 °	100 kV + coll 9 mm	7 mA	150179	114185	57952	-21958
-15 °	120 kV + coll 9 mm	8 mA	471462	394364	128523	-51425
-15 °	140 kV + coll 9 mm	9 mA	1005610	859694	236165	-90249
-15 °	160 kV + coll 9 mm	10 mA	1829913	1604745	401474	-176306
15 °	100 kV + coll 9 mm	7 mA	174544	117568	77688	-20712
15 °	120 kV + coll 9 mm	8 mA	526336	388903	172362	-34929

Angle axis-detector	Energy	Flow	Pierced Pb part + Fan blade	Environmental scattering	Secondary source scattering	Fan blade scattering
15 °	140 kV + coll 9 mm	9 mA	1104643	828012	315141	-38510
15 °	160 kV + coll 9 mm	10 mA	2004723	1519536	537435	-52248
45 °	100 kV + coll 9 mm	7 mA	103803	80467	17871	5465
45 °	120 kV + coll 9 mm	8 mA	410342	337608	43861	28873
45 °	140 kV + coll 9 mm	9 mA	943316	787090	88628	67598
45 °	160 kV + coll 9 mm	10 mA	1807051	1521294	158916	126841
75 °	100 kV + coll 9 mm	7 mA	112260	103455	5157	3648
75 °	120 kV + coll 9 mm	8 mA	493203	452525	11681	28997
75 °	140 kV + coll 9 mm	9 mA	1175527	1085348	5144	85035
75 °	160 kV + coll 9 mm	10 mA	2297535	2121401	22640	153494

Figure 15: fan blade scattering

Like in the previous case, the absolute values of the results got after subtraction could represent the fan blade scattering if there were no part filtering.
There are many positive results but less than in the titanium wedge case; this difference is the effect of geometry.

4.4.5 Scattering : data recapitulation

These are the scattering values got for the 4 parts tested:

Angle axis-detector	Energy	Flow	Environ. scattering	Secondary source scattering	Inco wedge scattering	Stiffener part scattering	Ti wedge scattering	Fan blade scattering
-75 °	100 kV	7 mA	110651	12653	-5544	-8425	-5569	-8078
-75 °	120 kV	8 mA	497666	35912	-20767	-24148	-19667	-24663
-75 °	140 kV	9 mA	1190728	74825	-48951	-47869	-37907	-49743
-75 °	160 kV	10 mA	2316141	141025	-102314	-100638	-77375	-104575
-45 °	100 kV	7 mA	86940	19424	-5662	-14887	2169	-2237
-45 °	120 kV	8 mA	374446	55118	-19428	-38109	3205	-7282
-45 °	140 kV	9 mA	881833	118551	-42432	-79714	-37	-23449
-45 °	160 kV	10 mA	1686811	225289	-92276	-158444	-17302	-58097
-15 °	100 kV	7 mA	114185	57952	-51174	-94458	-7373	-21958
-15 °	120 kV	8 mA	394364	128523	-116195	-210801	-20170	-51425
-15 °	140 kV	9 mA	859694	236165	-201658	-372094	-37870	-90249
-15 °	160 kV	10 mA	1604745	401474	-341067	-630056	-82565	-176306
15 °	100 kV	7 mA	117568	77688	-66021	-109628	7599	-20712
15 °	120 kV	8 mA	388903	172362	-141231	-232476	27855	-34929
15 °	140 kV	9 mA	828012	315141	-234255	-392110	65768	-38510
15 °	160 kV	10 mA	1519536	537435	-382209	-627100	115805	-52248
45 °	100 kV	7 mA	80467	17871	-1571	-10701	12090	5465
45 °	120 kV	8 mA	337608	43861	1117	-57727	42477	28873
45 °	140 kV	9 mA	787090	88628	6872	-22940	87454	67598
45 °	160 kV	10 mA	1521294	158916	6634	-30881	162266	126841
75 °	100 kV	7 mA	103455	5157	-656	-1546	7133	3648
75 °	120 kV	8 mA	452525	11681	-2244	3465	36566	28997
75 °	140 kV	9 mA	1085348	5144	-189	22385	95680	85035
75 °	160 kV	10 mA	2121401	22640	-13531	37983	174909	153494

Figure 17: scattering data recapitulation

5. Conclusion

Scattering of the x-ray photons by the test object constitutes one of the most important physical mechanisms having a significant impact on radiographic image. Many parameters of the radiographic scene may influence this scattered radiation :

- Distance object – detector

  More the object is closed to the detector, more the scattered radiation is important and can draw structures.

- Energy

  Influence on the scattering phenomena (Compton, Rayleigh, Photoelectric) and on the deviation of particles…

- Environment / Collimators

  Addition of the scattered coming from the environment of the scene (wall, detector, equipment set-up…). Collimators can reduce this problem…

- Materials object

The results of the several tests completed with the Canberra detector are a progress in the understanding of the scattered radiation phenomenon. The experimental tests have showed that the scattered radiation was influenced by the parts material (density differences) and geometry (simple or complex) put on the X-ray axis. The different positions of the detector tested have allowed to have an idea of its spatial distribution. At last it gives the capability to evaluate the different contributions (environment and part) to the scattered radiation.

6. Bibliography

1. SNECMA, doc n°2005/39, « Minutes of WP1 technical meeting set at Turboméca (Bordes) on the 27th of January 2005 », appendix 1 « Presentation of results of last experimental tests for validation (SNECMA) »
2. SNECMA, doc n°2005/85, « Minutes of WP1 technical meeting set at CEA-LETI (Grenoble) on the 29th of March 2005 », appendix 1 « Presentation of results of last experimental tests for validation (SNECMA) »